Electronic Supplementary Material (ESI) for Chemical Communications

Supporting Information for: Water soluble triazolopyridiniums as tunable blue light emitters

Xin Su[a], Matthew D. Liptak[b] and Ivan Aprahamian*[a]

[a] *Department of Chemistry, Dartmouth College, Hanover, New Hampshire 03755, USA.*

[b] *Department of Chemistry, University of Vermont, Burlington, Vermont 05405, USA.*

E-mail: ivan.aprahamian@dartmouth.edu
Website: www.dartmouth.edu/~aprahamian/

Electronic Supplementary Material (ESI) for Chemical Communications

Table of Contents

1 General

All reagents and starting materials were purchased from commercial sources and used as supplied unless otherwise indicated. All experiments were conducted in air unless otherwise noted. Column chromatography was performed on silica gel (SiliCycle®, 60 Å, 230-400 mesh). All solvent mixtures were reported as volume ratios unless otherwise noted. Deuterated solvents were purchased from Cambridge Isotope Laboratories, Inc. and used as received. NMR spectra were recorded on a Varian Mercury 300 MHz NMR spectrometer, with working frequencies of 299.97 MHz for ^{1}H nuclei and 75.44 MHz for ^{13}C nuclei, respectively, and a Varian Unity Plus 500 MHz NMR spectrometer, with working frequencies of 499.87 MHz for ^{1}H nuclei and 125.7 MHz for ^{13}C nuclei, respectively. Chemical shifts are quoted in ppm relative to tetramethylsilane (TMS), using the residual solvent peak as the reference standard. Mass spectra were obtained either on a Shimadzu GCMS-QP2010S gas chromatograph/EI mass spectrometer or on a Waters Quattro II ESI mass spectrometer. Melting points were measured on an Electrothermal Thermo Scientific IA9100X1 digital melting point instrument. UV-Vis spectra were recorded on a Shimadzu UV-1800 UV-Vis spectrophotometer. Solution fluorescence spectra were recorded on a Shimadzu RF-1501 fluorospectrophotometer with a slit width of 5 nm and a scanning speed of 200 nm·min^{-1}. Quinine sulfate dihydrate (std) was used as the fluorescence quantum yield reference ($\Phi = 0.54$, $\lambda_{ex} = 310$ nm, 5×10^{-4} M 0.01 M H_2SO_4).[S1] Quantum yields were determined using Equation S1,[S2] where Φ is the quantum yield, I is the integral of the emission peak, A denotes the absorbance at the excitation wavelength and n is the reflective index of the solvent.

$$\Phi = \Phi_{std}\frac{I\cdot A_{std}\cdot n^2}{I_{std}\cdot A\cdot n_{std}^2} \tag{S1}$$

2 Synthesis

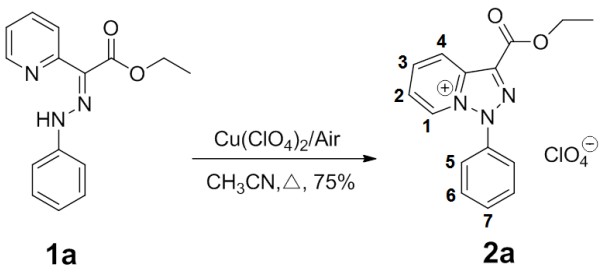

Scheme S1: The synthesis of **2a**.

1a was synthesized following a reported procedure.[S3]

2a: **1a** (0.269 g, 0.001 mol) was dissolved in 5 mL acetonitrile (CH_3CN) and the well stirred solution was heated to 60 °C. Copper(II) perchlorate hexahydrate ($Cu(ClO_4)_2 \cdot 6H_2O$) (0.741 g, 0.002 mol; 2 equiv.) was then added to the solution. The reaction mixture was kept at 60 °C overnight. The reaction mixture was then filtered, and 30 mL 5% (wt.) perchloric acid ($HClO_4$) solution was added to the filtrate. The precipitate was collected by filtration and subjected to recrystallization from acetonitrile and 5% (wt.) $HClO_4$ solution. **2a** was obtained as a light yellow powder (0.276 g, 75%); m.p.: decomposes > 220 °C; ^{1}H NMR (500 MHz, CD_3CN) δ 8.98 (dd, *J*= 7.1, 0.5 Hz, H1), 8.81 (dd, *J*= 8.8, 1.1 Hz, H4), 8.36 (dd, *J*= 8.3, 7.7 Hz, H2), 8.02 – 7.94 (m, H3), 7.90 (tdd, *J*= 10.4, 5.1, 2.9 Hz, H7), 7.87 – 7.80 (m, H5, H6), 4.61 (q, *J*= 7.1 Hz, –CH_2–), 1.49 (t, *J*= 7.1 Hz, –CH_3) ppm; ^{13}C NMR (75 MHz, CD_3CN) δ 159.06, 137.92, 136.69, 134.61, 134.31, 134.28, 133.48, 132.14, 127.96, 125.59, 125.22, 122.43, 110.60, 64.26, 14.33 ppm. MS (ESI): *m/z* found [M^+] for $C_{15}H_{14}N_3O_2^+$ 268.2 (calcd. 268.3).

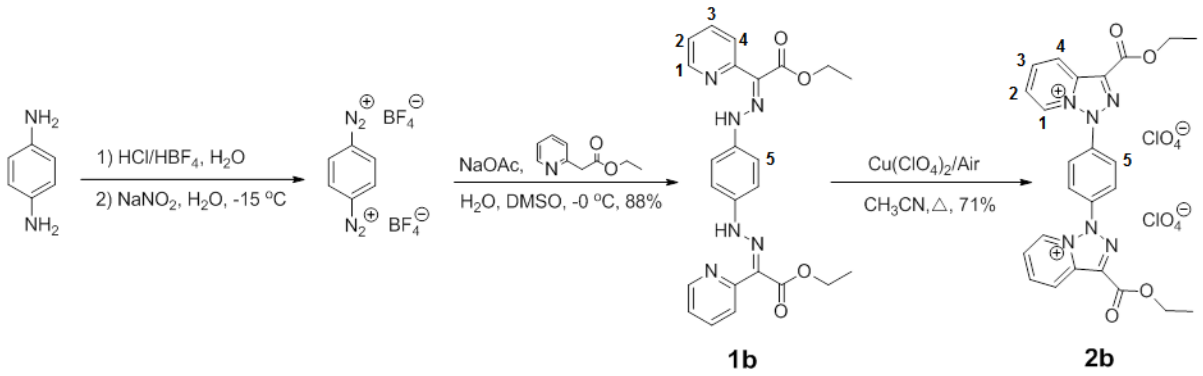

Scheme S2: The synthesis of **1b** and **2b**.

1b: The diazotiation procedure of 1,4-phenylenediamine was modified from a previsouly reported method.[S4] 1,4-phenylenediamine (0.54 g, 0.005 mol) was suspended in 2.5 mL concentrated hydrochloric acid (HCl) and was cooled to −15 °C using a dry ice/benzyl alcohol bath. A solution of 4 mL concentrated HCl and 4 mL 40% fluoroboric acid (HBF_4) was precooled to −15 °C and added dropwise to the suspension. After 15 min, a cold solution (2 mL) of sodium nitrite ($NaNO_2$, 1.38 g, 0.02mol; 4 equiv.) was added dropwise to the suspension. After stirring for 1 h, the diazonium salt was collected by filtration. After washing with a small amount of water, the diazonium salt was added in small portions to a suspension of ethyl-2-pyridylacetate (1.5 mL, 0.01 mol; 2 equiv.) and sodium acetate (5.01 g, 0.032 mol; 6.4 equiv.) in an ice bath-cooled solution of 9 mL dimethyl sulfoxide (DMSO) and 15 mL water. The reaction mixture was stirred overnight, during which the product precipitated out. The precipitate was collected by filtration, re-dissolved in methylene chloride (CH_2Cl_2), washed twice with 30 mL saturated potassium bicarbonate (K_2CO_3) solution and dried over magnesium sulfate ($MgSO_4$). The crude product was then subjected to silica gel column chromatography (ethyl acetate/hexane 1:5) to give **1b** as a dark yellow powder (2.20 g, 88%) m.p. 155.1 – 155.5 °C; ^{1}H NMR (300 MHz, $CDCl_3$) δ 14.98 (s, N–H), 8.71 – 8.60 (m, H1), 8.28 (d, J= 8.4 Hz, H4), 7.85 – 7.76 (m, H3), 7.39 (s, H5), 7.31 – 7.21 (2m, H2), 4.38 (q, J= 7.1 Hz, –CH_2–), 1.45 (t, J= 7.1 Hz, –CH_3) ppm; ^{13}C NMR (75 MHz, $CDCl_3$) δ 165.92, 153.11, 146.39, 139.24, 136.85, 124.78, 124.32, 122.15, 116.13, 61.08, 14.58 ppm. MS (EI): m/z found [M^+] for $C_{24}H_{24}N_6O_4^+$ 460 (calcd. 460).

2b: **2b** was synthesized following a similar procedure to **2a**, but 4 equiv. of $Cu(ClO_4)_2 \cdot 6H_2O$ was used instead of 2 equiv. **2b** was obtained as a yellow powder in 71% yield, m.p. decomposes > 220 °C; ^{1}H NMR (300 MHz, CD_3CN) δ 9.21 (d, J= 7.1 Hz, H1), 8.89 (dt, J= 8.8, 1.1 Hz, H4), 8.45 (ddd, J= 8.8, 7.2, 0.8 Hz, H3), 8.30 (s, H5), 8.09 (td, J= 7.1, 1.3 Hz, H2), 4.64 (q, J= 7.1 Hz, –CH_2–), 1.51 (t, J= 7.1 Hz, –CH_3) ppm; ^{13}C NMR (75 MHz, CD_3CN) δ 158.11, 137.97, 136.23, 134.56, 130.52, 125.23, 125.11, 122.09, 63.80, 13.60 ppm. MS (ESI): M^+ for $C_{24}H_{22}{}^{35}ClN_6O_8^+$ 557.1 (calcd. 557.1) and $C_{24}H_{22}{}^{37}ClN_6O_8^+$ 559.1 (calcd. 559.1).

The ^{1}H NMR spectrum of **2a** shows that all aromatic signals are shifted downfield relative to the parent hydrazone, which is consistent with the development of a positive charge in the pyridyl ring.[S3] This effect is more pronounced in **2b**, where the phenyl proton signal is shifted downfield to 8.33 ppm as opposed to 7.38 ppm in **1b**. Moreover, the spectrum does not contain the hydrazone N–H proton, which is an indication that the oxidative cyclization has taken place.

3 Photophysical Properties

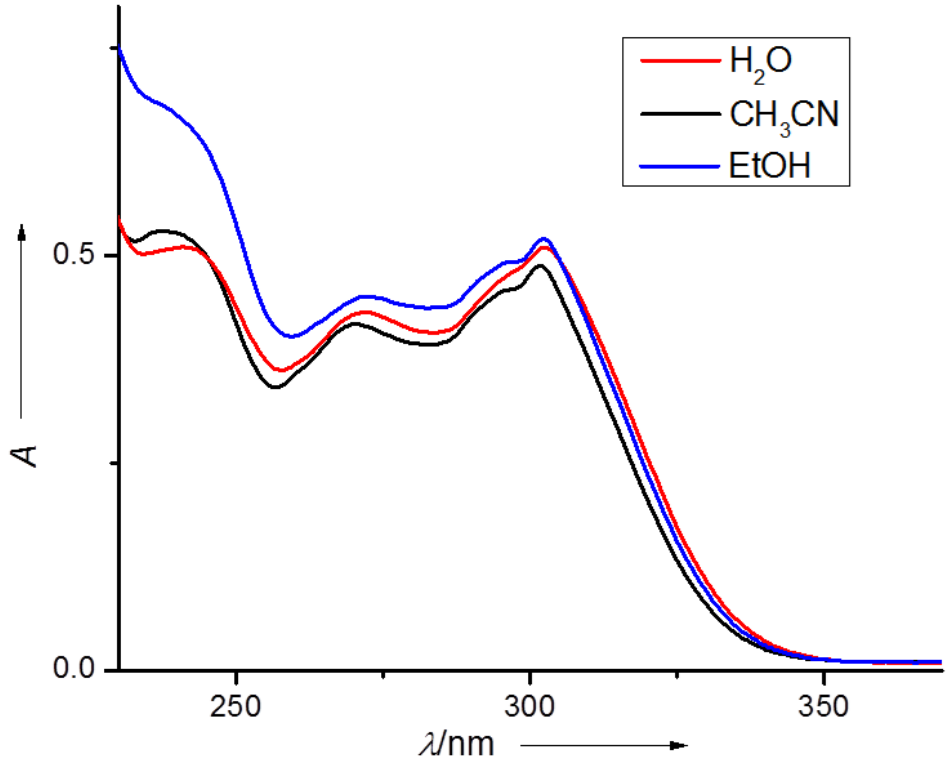

Figure S1: UV-vis absorption spectra of **2a** (5.0×10^{-5} M) in H_2O, CH_3CN and EtOH.

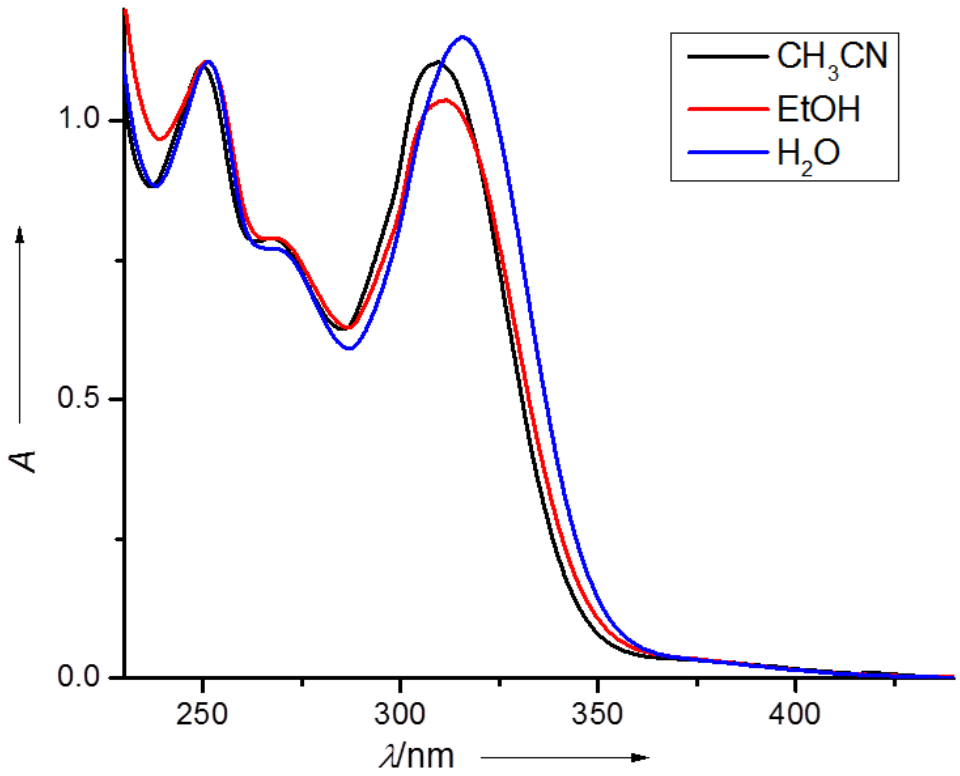

Figure S2: UV-vis absorption spectra of **2b** (5.0×10^{-5} M) in H_2O, CH_3CN and EtOH.

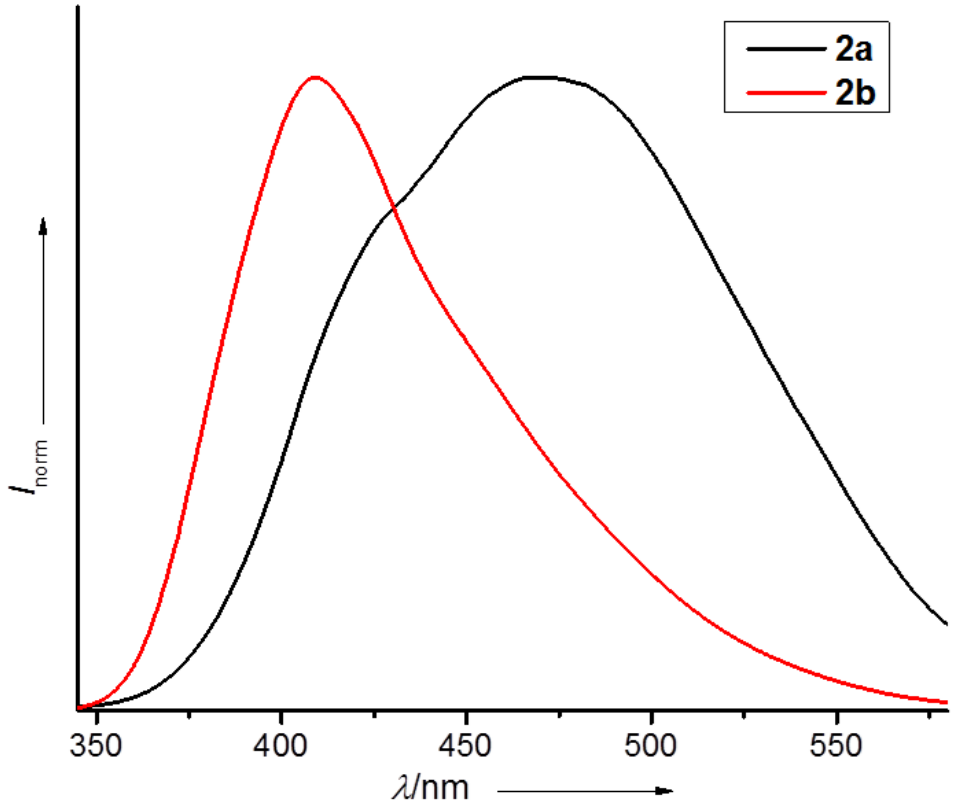

Figure S3: Normalized fluorescence spectra of **2a** and **2b** (both 1.0×10^{-5} M) in CH_3CN.

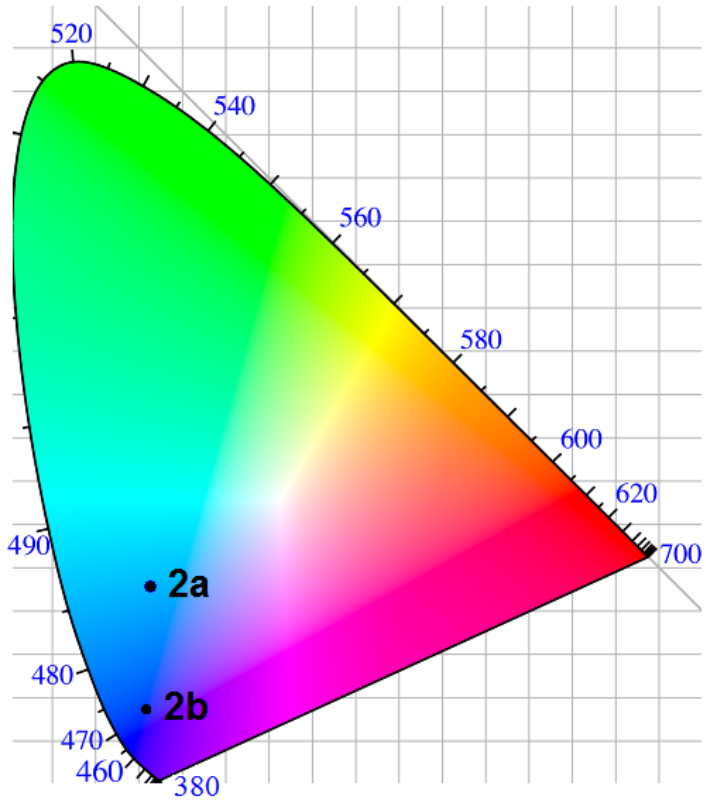

Figure S4: The coordinates of **2a** (0.159, 0.232) and **2b** (0.159, 0.094) in the CIE (Commission internationale de l'éclairage) 1931 color space chromaticity diagram,[S5] calculated from their emission profiles in H_2O.

4 Single Crystal Diffraction

Data were collected using a Bruker CCD (charge coupled device) based diffractometer equipped with an Oxford Cryostream low-temperature apparatus operating at 173 K. Data were measured using ω and ϕ scans of 0.5° per frame for 30 s. The total number of images was based on results from the program COSMO[S6] where redundancy was expected to be 4.0 and completeness of 100% out to 0.83 Å. Cell parameters were retrieved using APEX II software[S7] and refined using SAINT on all observed reflections. Data reduction was performed using the SAINT software[S8] which corrects for L_p. Scaling and absorption corrections were applied using SADABS[S9] multi-scan technique, supplied by George Sheldrick. The structures are solved by the direct method using the SHELXS-97 program and refined by least squares method on F^2, SHELXL-97, which are incorporated in SHELXTL-PC V 6.10.[S10] All non-hydrogen atoms are refined anisotropically. All hydrogens were calculated by geometrical methods and refined as a riding model.

Table S1: Crystal Data and Parameters for **2a**.

	2a
CCDC	887676
Empirical formula	$C_{15}H_{14}ClN_3O_6$
Formula weight	367.74
Temperature	173(2) K
Wavelength	0.71073 Å
Crystal system	Monoclinic
Space group	$P2_1/n$
Unit cell dimensions	a = 13.7923(7) Å
	$\alpha = 90°$
	b = 5.9508(3) Å
	β = 100.5400(10)°
	c = 19.9335(11) Å
	$\gamma = 90°$
Volume	1608.44(15) Å^3
Z	4
Density (calcd.)	1.519 Mg·m^{-3}
Absorption coefficient	0.277 mm^{-1}
$\boldsymbol{F}_{000}$	760
Crystal size	0.49 × 0.33 × 0.04 mm^3
θ range for data collection	1.66 to 25.39°
Index ranges	-16 ≤ h ≤ 16
	-7 ≤ k ≤ 7
	-24 ≤ l ≤ 24
Reflections collected	24909
Independent reflections	2947 [R_{int} = 0.0287]
Completeness to θ = 25.36°	100.0%
Absorption correction	Semi-empirical from equivalents
Max. and min. transmission	0.9896 and 0.8758
Refinement method	Full-matrix least-squares on F^2
Data / restraints / parameters	2947 / 0 / 254
Goodness-of-fit on F^2	1.047
Final R indices [$I > 2\sigma(I)$]	R_1 = 0.0401, ωR_2 = 0.1110
R indices (all data)	R_1 = 0.0468, ωR_2 = 0.1178
Largest diff. peak and hole	0.422 and -0.332 e·Å^{-3}

5 Density Functional Theory Calculations

The electronic structure calculations presented in this work were performed using the ORCA 2.9.1 software package on the 364 node IBM cluster at the Vermont Advanced Computing Core (VACC).[S11] Each density functional theory calculation utilized the PBE density functional,[S12] the TZVP basis set,[S13] and tight SCF convergence criteria. Geometry optimizations of **2a** and **2b** (Fig. S5) were performed in the presence of a COSMO continuum solvation model with $\varepsilon = 36.6$ and $\eta = 1.344$ (CH_3CN) or $\varepsilon = 80.4$ and $\eta = 1.33$ (H_2O).[S14]

Time-dependent density functional theory (TDDFT) was used to calculate the energies and UV/Vis absorption intensities of a total of 20 excited states within an expansion space of 120 vectors for both the CH_3CN and H_2O models. The UV/Vis absorption spectra of **2a** and **2b** in CH_3CN and H_2O were simulated using the orca_mapspc utility program with full width at half maximum bandwidths of 2500 cm^{-1} (Fig. S6). In all four cases, the primary contribution to the lowest energy (longest wavelength) TDDFT transition with significant UV/Vis intensity is a one-electron excitation from the ground state HOMO to the ground state LUMO. The molecular orbital and TDDFT difference plots were drawn in gOpenMol with isodensity values of $\pm$ 0.03 au and $\pm$ 0.003 au, respectively (Figs. 3 and S7–S8).[S15]

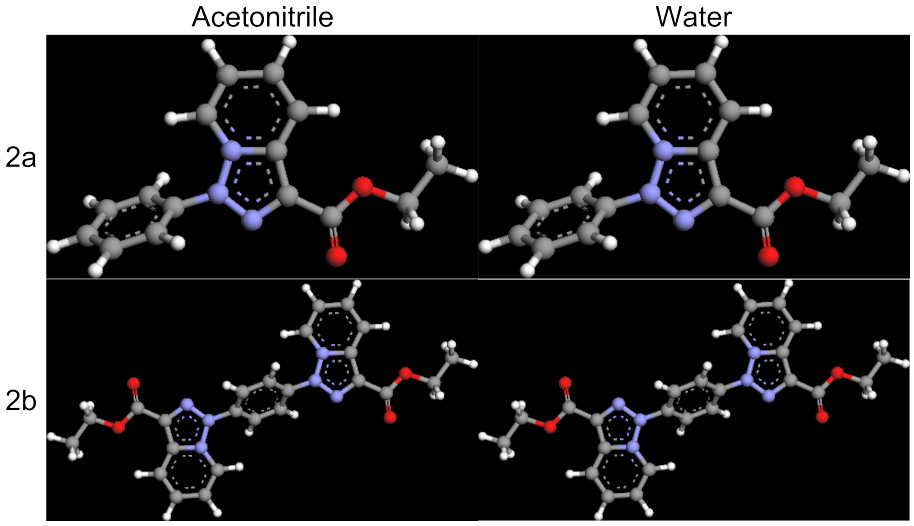

Figure S5: Ball-stick drawing of the COSMO/PBE/TZVP structures of **2a** and **2b** in CH_3CN and H_2O.

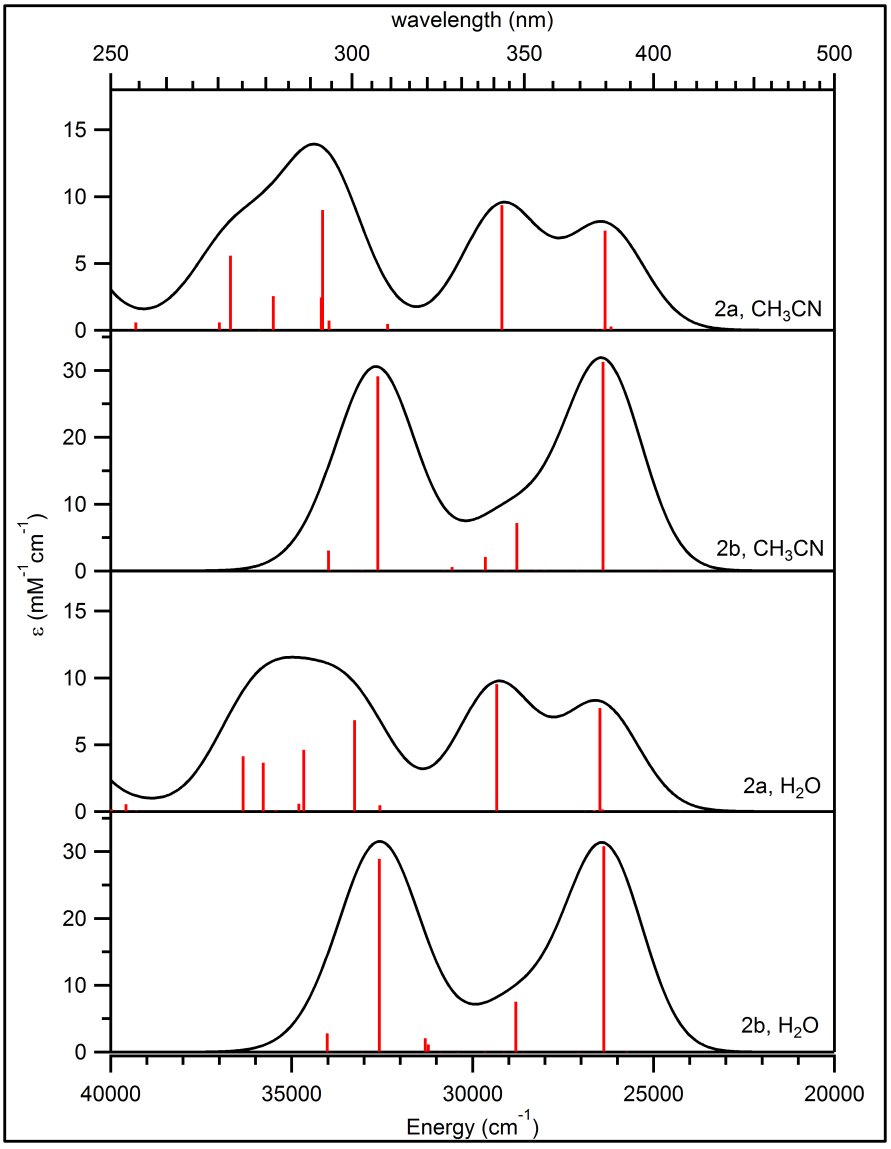

Figure S6: TDDFT-computed UV/Vis absorption spectra of **2a** and **2b** in CH_3CN and H_2O.

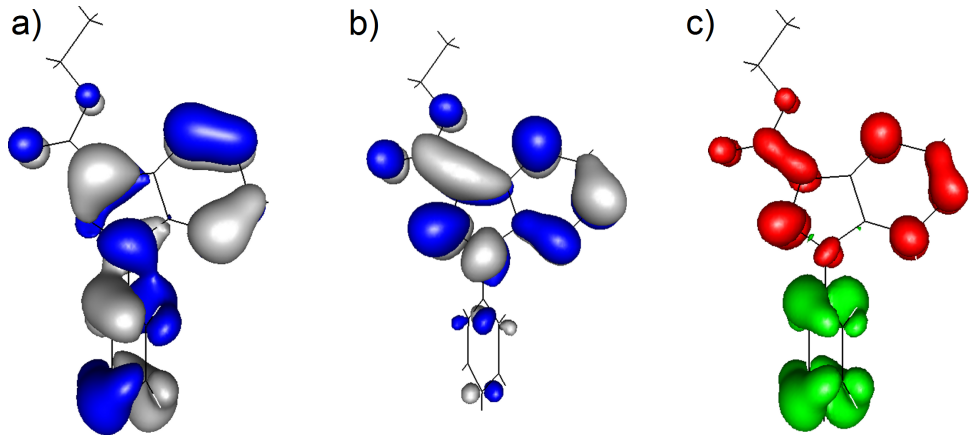

Figure S7: COSMO/PBE/TZVP TDDFT-computed a) HOMO, b) LUMO, and c) TDDFT difference density of **2a** in CH_3CN. Green indicates a loss of electron density upon excitation at 380 nm and red indicates a gain of electron density.

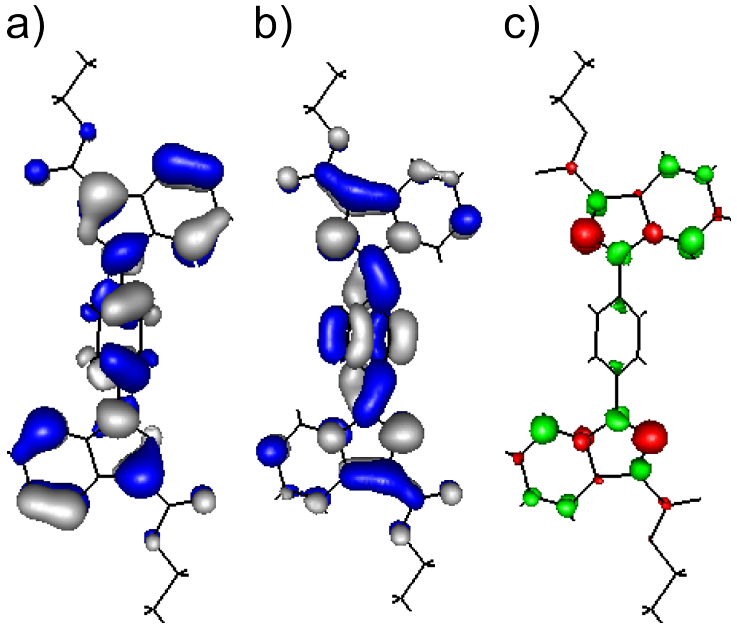

Figure S8: COSMO/PBE/TZVP TDDFT-computed a) HOMO, b) LUMO, and c) TDDFT difference density of **2b** in CH_3CN. Green indicates a loss of electron density upon excitation at 380 nm and red indicates a gain of electron density.

Table S2: Cartesian Coordinates for the COSMO/PBE/TZVP Model of **2a** in CH_3CN.

C	0.504768	-1.909638	1.109717
C	0.492022	-3.298746	1.247867
C	0.010349	-4.104913	0.210441
C	-0.459688	-3.529346	-0.975532
C	-0.441889	-2.143363	-1.138885
C	0.041725	-1.357438	-0.089023
N	0.028662	0.068314	-0.246902
N	1.157399	0.861496	-0.231756
C	0.747654	2.162401	-0.459720
C	1.722323	3.171905	-0.486815
C	3.045802	2.816587	-0.298878
C	3.409175	1.465967	-0.089997
C	2.456502	0.476080	-0.054752
C	-0.664672	2.060856	-0.624911
C	-1.677753	3.114224	-0.894596
N	-1.047807	0.789631	-0.490697
O	-1.091137	4.318899	-0.970992
O	-2.869120	2.888052	-1.022621
C	-1.979355	5.464141	-1.226778
C	-1.118377	6.703900	-1.278578
H	0.847197	-1.269778	1.924236
H	0.845965	-3.748787	2.176263
H	-0.002755	-5.189892	0.329070
H	-0.836254	-4.160208	-1.781862
H	-0.795705	-1.675828	-2.058210
H	1.412882	4.200052	-0.659929
H	3.820729	3.582692	-0.317160
H	4.452053	1.183602	0.047078
H	2.652636	-0.582924	0.096181
H	-2.503734	5.278835	-2.174575
H	-2.719475	5.503409	-0.414805
H	-1.762466	7.574836	-1.465583
H	-0.593730	6.865985	-0.326641
H	-0.379858	6.644024	-2.090372

Table S3: Cartesian Coordinates for the COSMO/PBE/TZVP Model of **2a** in H_2O.

C	0.505570	-1.909478	1.109073
C	0.492725	-3.298605	1.247252
C	0.010147	-4.104767	0.210221
C	-0.460574	-3.529153	-0.975498
C	-0.442655	-2.143160	-1.138890
C	0.041668	-1.357289	-0.089310
N	0.028672	0.068401	-0.247222
N	1.157274	0.861653	-0.231674
C	0.747610	2.162548	-0.459483
C	1.722139	3.172049	-0.486255
C	3.045584	2.816658	-0.297990
C	3.408872	1.466104	-0.089141
C	2.456198	0.476183	-0.054314
C	-0.664702	2.060893	-0.624867
C	-1.677618	3.114034	-0.894195
N	-1.047841	0.789629	-0.490926
O	-1.091550	4.318600	-0.971311
O	-2.869440	2.887859	-1.021499
C	-1.979521	5.463971	-1.226844
C	-1.118045	6.703362	-1.279398
H	0.849118	-1.269641	1.923116
H	0.847584	-3.748600	2.175324
H	-0.002872	-5.189763	0.328836
H	-0.837501	-4.159974	-1.781705
H	-0.796404	-1.675606	-2.058230
H	1.413035	4.200287	-0.659315
H	3.820497	3.582764	-0.315993
H	4.451664	1.183666	0.048274
H	2.652556	-0.582763	0.096581
H	-2.504361	5.278755	-2.174405
H	-2.719052	5.503840	-0.414363
H	-1.761957	7.574474	-1.466241
H	-0.592775	6.865273	-0.327776
H	-0.379981	6.642821	-2.091549

Table S4: Cartesian Coordinates for the COSMO/PBE/TZVP Model of **2b** in CH_3CN.

C	1.193886	0.738247	0.635088
C	1.219218	-0.652718	0.680313
C	0.247497	-1.367864	-0.027095
C	-0.744588	-0.734633	-0.780924
C	-0.769954	0.656316	-0.826090
C	0.201791	1.371447	-0.118718
N	0.173319	2.800463	-0.120516
N	0.173783	3.590702	-1.252134
C	0.161462	4.906732	-0.826102
C	0.158807	5.921419	-1.793970
C	0.187348	5.560172	-3.129427
C	0.228979	4.199185	-3.507695
C	0.223210	3.201951	-2.561416
C	0.177073	4.817470	0.598004
C	0.179146	5.890715	1.628837
N	0.186495	3.540027	0.973709
O	0.152561	7.097128	1.044790
O	0.203336	5.671299	2.827457
C	0.154315	8.261962	1.944778
C	0.136780	9.501771	1.082842
H	1.947437	1.322463	1.162246
H	2.011534	-1.162758	1.228278
H	-1.498247	-1.318872	-1.307890
H	-1.562219	1.166433	-1.374063
H	0.142018	6.959547	-1.470203
H	0.187766	6.330848	-3.899917
H	0.270122	3.911992	-4.557457
H	0.266495	2.137052	-2.776634
H	-0.732383	8.188473	2.590261
H	1.055180	8.201042	2.571513
H	0.137223	10.386508	1.735144
H	1.025556	9.553132	0.438188
H	-0.765410	9.540607	0.456285
N	0.275660	-2.796893	-0.025412
N	0.274365	-3.587397	1.106053
C	0.283990	-4.903354	0.679679
C	0.284964	-5.918285	1.647298
C	0.257851	-5.557314	2.982868
C	0.219008	-4.196349	3.361492
C	0.226336	-3.198887	2.415450
C	0.268006	-4.813743	-0.744395
C	0.264296	-5.886736	-1.775484
N	0.260627	-3.536208	-1.119793
O	0.284761	-7.093381	-1.191661
O	0.243913	-5.666946	-2.974103
C	0.281971	-8.257976	-2.091956
C	0.289487	-9.498071	-1.230298
H	0.299605	-6.956366	1.323264
H	0.256250	-6.328216	3.753133
H	0.178755	-3.909348	4.411340
H	0.184581	-2.133982	2.630919
H	1.172295	-8.188483	-2.732877
H	-0.615365	-8.192668	-2.723292
H	0.289004	-10.382610	-1.882864
H	-0.603060	-9.545856	-0.590619
H	1.188007	-9.540907	-0.598720

Table S5: Cartesian Coordinates for the COSMO/PBE/TZVP Model of **2a** in H_2O.

C	1.195441	0.737422	0.634044
C	1.220856	-0.653569	0.677602
C	0.247879	-1.367655	-0.029034
C	-0.745600	-0.733832	-0.780389
C	-0.770976	0.657136	-0.823996
C	0.201982	1.371208	-0.117322
N	0.173614	2.800255	-0.118420
N	0.174536	3.590192	-1.250113
C	0.161888	4.906312	-0.824697
C	0.159598	5.920497	-1.793000
C	0.188688	5.558472	-3.128239
C	0.230459	4.197351	-3.505803
C	0.224400	3.200631	-2.559010
C	0.176585	4.817357	0.599379
C	0.177626	5.890634	1.629476
N	0.185925	3.539909	0.975500
O	0.151922	7.096977	1.045449
O	0.200360	5.672091	2.828647
C	0.152704	8.261968	1.944771
C	0.136223	9.501330	1.082090
H	1.950154	1.320972	1.160240
H	2.013852	-1.164377	1.223820
H	-1.500440	-1.317412	-1.306354
H	-1.563885	1.168036	-1.370256
H	0.142603	6.958866	-1.470103
H	0.189391	6.328747	-3.899109
H	0.271947	3.909520	-4.555346
H	0.267705	2.135621	-2.773651
H	-0.734810	8.189132	2.589221
H	1.052921	8.201593	2.572508
H	0.135984	10.386445	1.733900
H	1.025700	9.552014	0.438348
H	-0.765221	9.539621	0.454421
N	0.275854	-2.796712	-0.027895
N	0.274612	-3.586749	1.103759
C	0.283975	-4.902847	0.678196
C	0.285053	-5.917133	1.646388
C	0.258383	-5.555184	2.981704
C	0.219954	-4.194024	3.359450
C	0.227156	-3.197221	2.412741
C	0.267851	-4.813759	-0.745846
C	0.264109	-5.886958	-1.776019
N	0.260725	-3.536276	-1.121860
O	0.283998	-7.093437	-1.192048
O	0.244292	-5.668232	-2.975208
C	0.281374	-8.258332	-2.091492
C	0.288479	-9.497846	-1.228913
H	0.299472	-6.955501	1.323365
H	0.256879	-6.325573	3.752462
H	0.180155	-3.906211	4.409061
H	0.185716	-2.132168	2.627522
H	1.171987	-8.189644	-2.732113
H	-0.615822	-8.193619	-2.723110
H	0.288127	-10.382864	-1.880850
H	-0.604251	-9.544826	-0.589429
H	1.186752	-9.540064	-0.596933

6 NMR Spectra

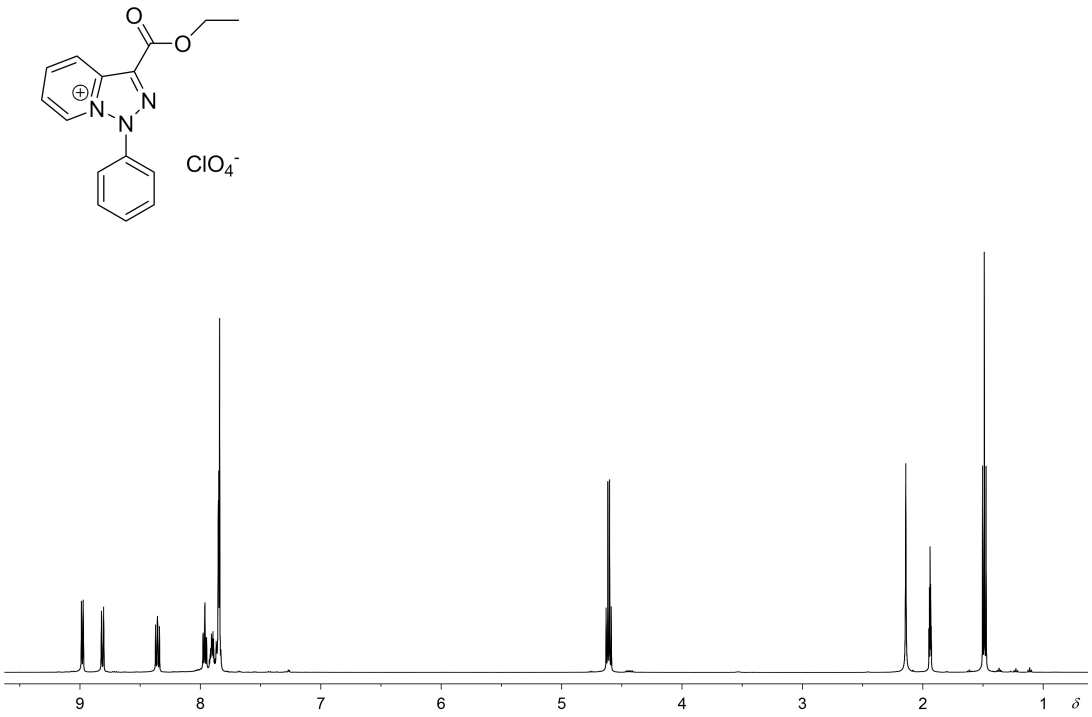

Figure S9: ^{1}H NMR spectrum of **2a** in CD_3CN at 294 K.

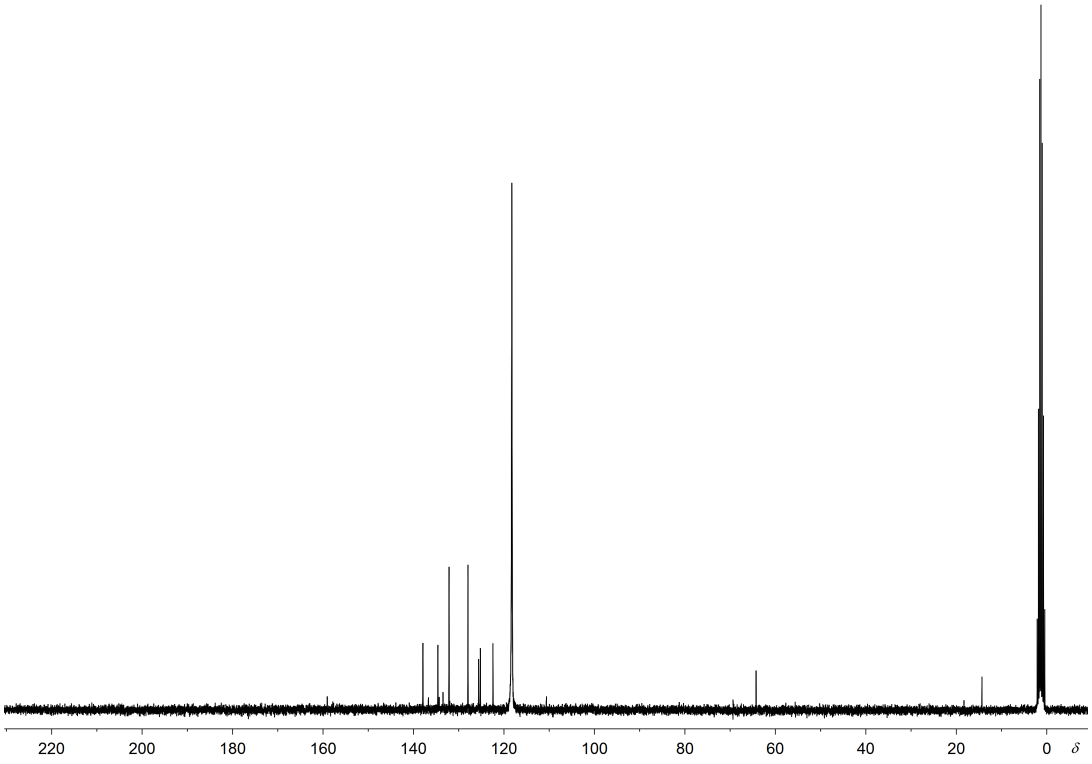

Figure S10: ^{13}C NMR spectrum of **2a** in CD_3CN at 294 K.

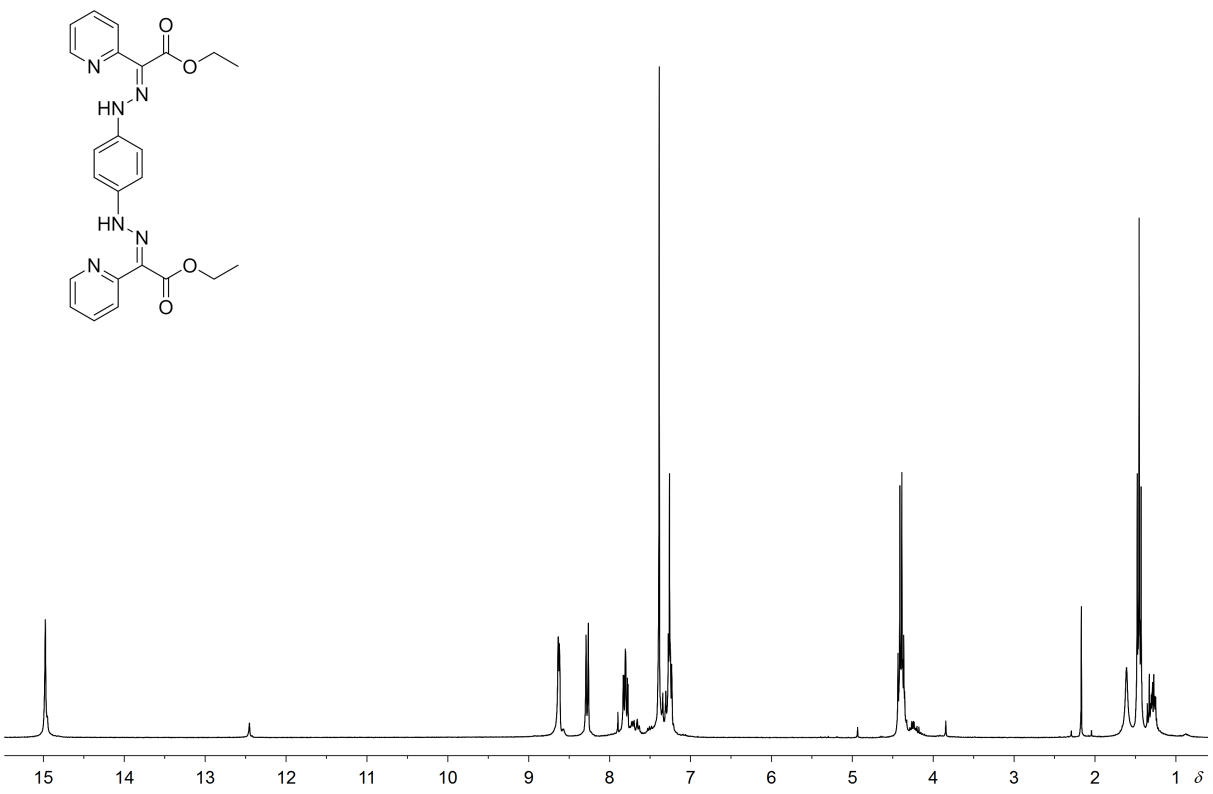

Figure S11: ^{1}H NMR spectrum of **1b** in $CDCl_3$ at 294 K in the presence of the minor *Z* isomer.

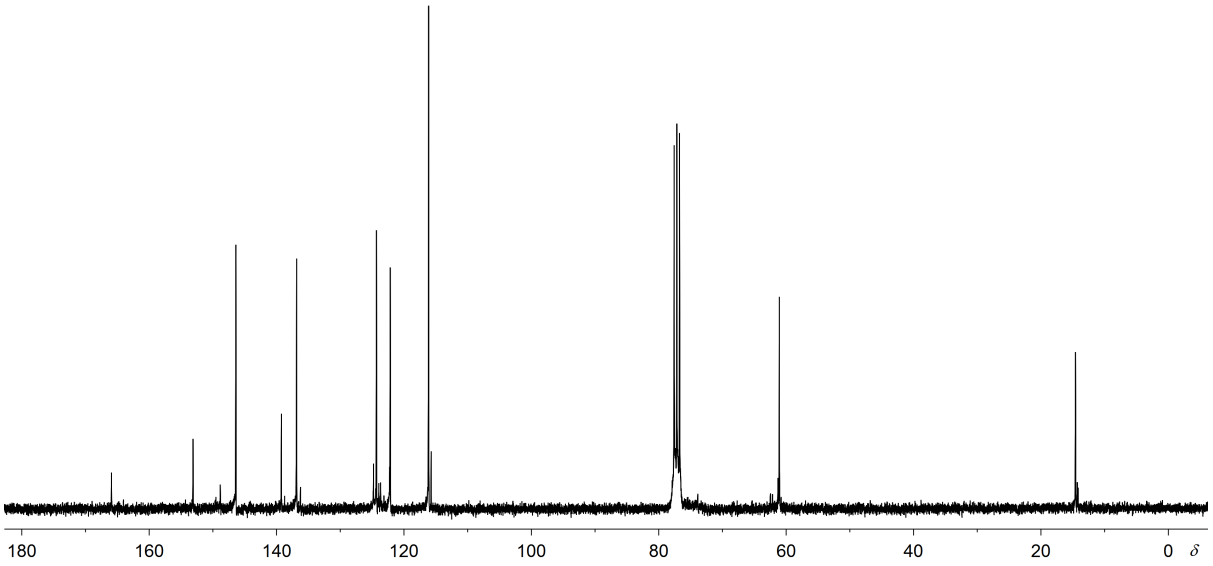

Figure S12: ^{13}C NMR spectrum of **1b** in $CDCl_3$ at 294 K in the presence of the minor *Z* isomer.

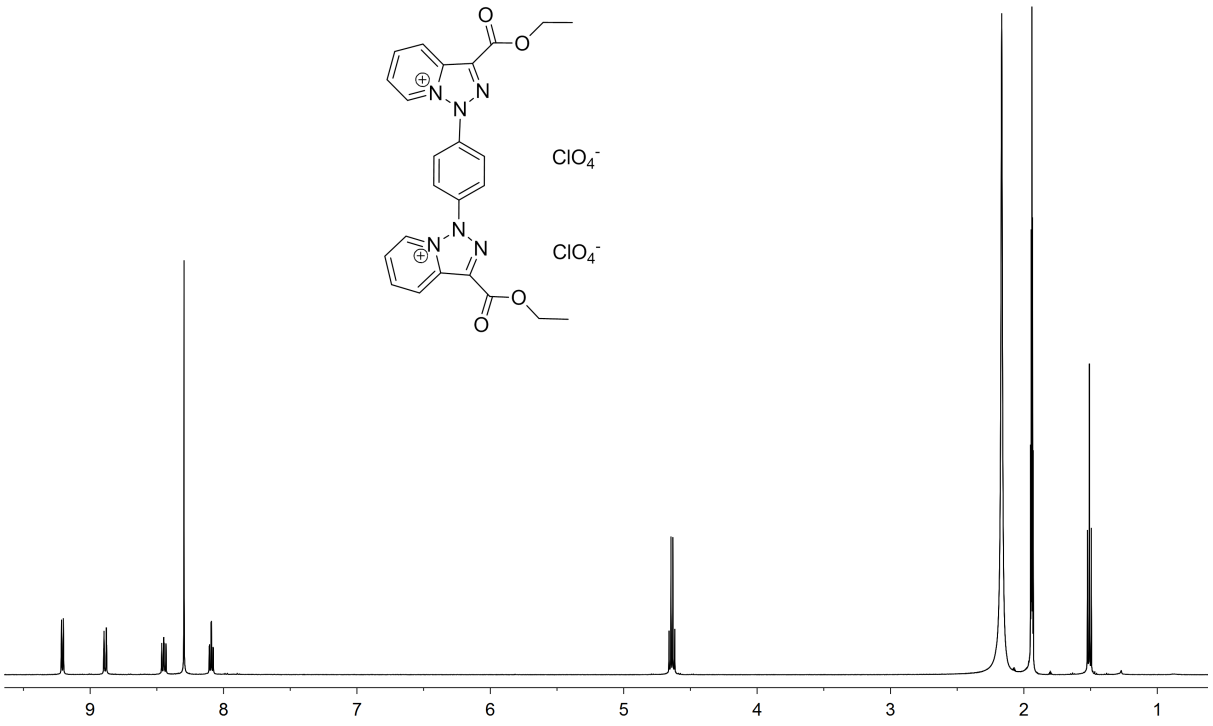

Figure S13: ^{1}H NMR spectrum of **2b** in CD_3CN at 294 K.

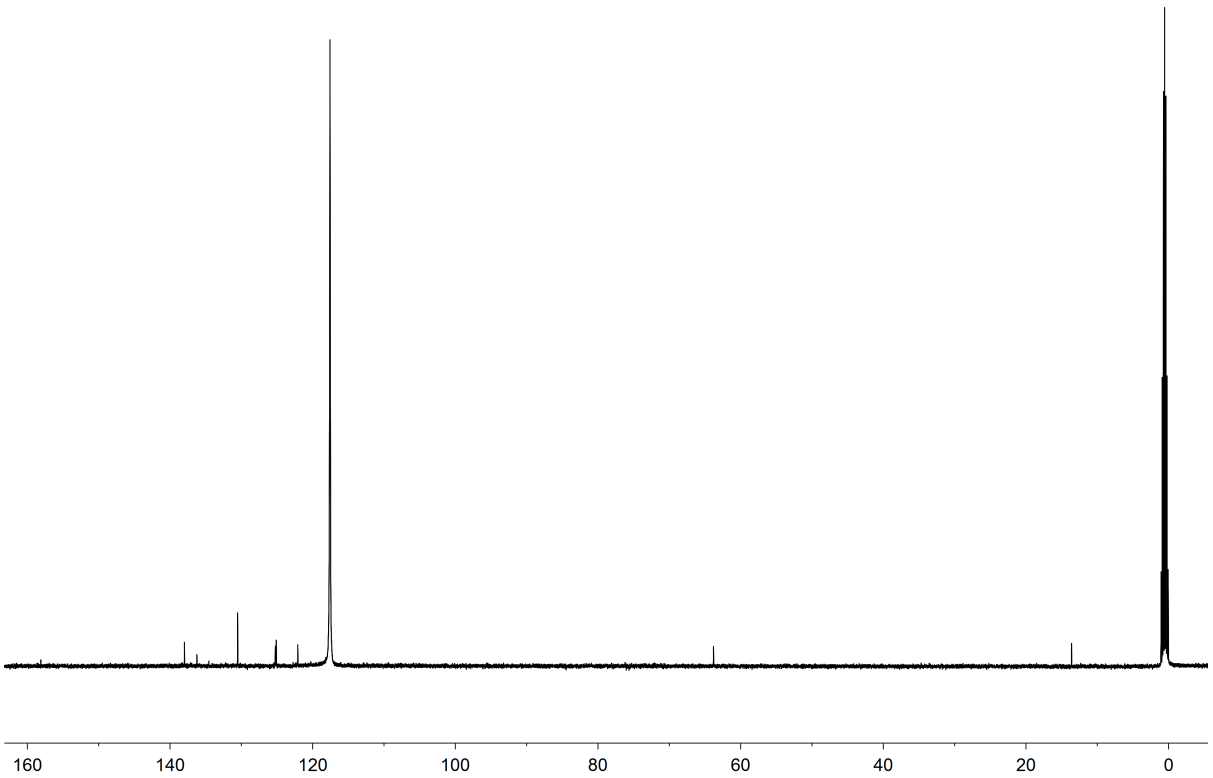

Figure S14: ^{13}C NMR spectrum of **2b** in CD_3CN at 294 K.

References

(S1) Melhuish, W. H. Quantum Efficiencies of Fluorescence of Organic Substances: Effect of Solvent and Concentration of the Fluorescent Solute. *J. Phys. Chem.* **1961**, *65*, 229–235.

(S2) Lakowicz, J. R. *Principles of Fluorescence Spectroscopy*, 3rd ed.; Springer: New York, USA, 2006.

(S3) Landge, S. M.; Tkatchouk, E.; Benítez, D.; Lanfranchi, D. A.; Elhabiri, M.; Goddard, W. A., III; Aprahamian, I. Isomerization Mechanism in Hydrazone-Based Rotary Switches: Lateral Shift, Rotation, or Tautomerization? *J. Am. Chem. Soc.* **2011**, *133*, 9812–9823.

(S4) Zeng, X.-W.; Huang, N.; Xu, H.; Yang, W.-B.; Yang, L.-M.; Qu, H.; Zheng, Y.-T. Anti Human Immunodeficiency Virus Type 1 (HIV-1) Agents 4. Discovery of 5,5'-(p-Phenylenebisazo)-8-hydroxyquinoline Sulfonates as New HIV-1 Inhibitors in Vitro. *Chem. Pharm. Bull.* **2010**, *58*, 976–979.

(S5) Patil, P. CIE Coordinate Calculator. 2010.

(S6) COSMO V1.58, Software for the CCD Detector Systems for Determining Data Collection Parameters. Bruker Analytical X-ray Systems: Madison, WI, USA, 2008.

(S7) APEX2 V2008.5-0 Software for the CCD Detector System. Bruker Analytical X-ray Systems: Madison, WI, USA, 2008.

(S8) SAINT V 7.34 Software for the Integration of CCD Detector System. Bruker Analytical X-ray Systems: Madison, WI, USA, 2008.

(S9) Blessing, R. H. An empirical correction for absorption anisotropy. *Acta Cryst. A* **1995**, *51*, 33–38.

(S10) Sheldrick, G. M. A short history of *SHELX*. *Acta Cryst. A* **2008**, *64*, 112–122.

(S11) Neese, F. ORCA 2.9.1. Max Planck Institute for Bioinorganic Chemistry: Mülheim, Germany, 2012.

(S12) Perdew, J. P.; Burke, K.; Ernzerhof, M. Generalized Gradient Approximation Made Simple. *Phys. Rev. Lett.* **1996**, *77*, 3865–3868.

(S13) Schäfer, A.; Horn, H.; Ahlrichs, R. Fully Optimized Contracted Gaussian Basis Sets for Atoms Li to Kr. *J. Chem. Phys.* **1992**, *97*, 2571–2577.

(S14) Sinnecker, S.; Rajendran, A.; Klamt, A.; Diedenhofen, M.; Neese, F. Calculation of Solvent Shifts on Electronic g-Tensors with the Conductor-Like Screening Model (COSMO) and Its Self-Consistent Generalization to Real Solvents (Direct COSMO-RS). *J. Phys. Chem. A* **2006**, *110*, 2235–2245.

(S15) Laaksonen, L. gOpenMol 2.32. Center for Scientific Computing: Espoo, Finland, 2003.